Room Temperature Giant and Linear Magnetoresistance in Topological Insulator Bi_2Te_3 Nanosheets

Xiaolin Wang,* Yi Du, Shixue Dou, and Chao Zhang

Institute for Superconducting and Electronic Materials, Faculty of Engineering, Australian Institute for Innovative Materials, University of Wollongong, NSW 2522, Australia

(Received 4 December 2011; published 29 June 2012)

Topological insulators, a new class of condensed matter having bulk insulating states and gapless metallic surface states, have demonstrated fascinating quantum effects. However, the potential practical applications of the topological insulators are still under exploration worldwide. We demonstrate that nanosheets of a Bi_2Te_3 topological insulator several quintuple layers thick display giant and linear magnetoresistance. The giant and linear magnetoresistance achieved is as high as over 600% at room temperature, with a trend towards further increase at higher temperatures, as well as being weakly temperature-dependent and linear with the field, without any sign of saturation at measured fields up to 13 T. Furthermore, we observed a magnetic field induced gap below 10 K. The observation of giant and linear magnetoresistance paves the way for 3D topological insulators to be useful for practical applications in magnetoelectronic sensors such as disk reading heads, mechatronics, and other multifunctional electromagnetic applications.

DOI: 10.1103/PhysRevLett.108.266806 PACS numbers: 73.43.Qt, 72.20.My, 73.63.−b

Topological insulators (TIs) represent a new class of condensed matter that has revealed unusual quantum phenomena [1–8]. The electrons are delocalized at the edges or surfaces but localized at the surface or inside the bulk in two- or three-dimensional (2D or 3D) TIs, respectively. The band structures of the surface states show a gapless linear energy dispersion in 3D TIs. In 3D TIs such as Bi_2Te_3 [9], free electrons at the surface have a helical spin configuration, and their spins are locked to their momentum due to strong spin-orbital coupling, resulting in net magnetic moments which can be generated by passing an in-plane current. The locking of spin and orbital states is protected by time-reversal symmetry, which means that the delocalized surface states are insensitive to defects, nonmagnetic dopants, or any environmental disturbances. These features have led to the discovery of spin Hall effects [2,3], the absence of backscattering from nonmagnetic impurities [10], topological superconductivity [11,12], the possible existence of Majorana fermions [13], and magnetoelectric quantum states [8]. So far, studies of the TIs have been mainly focused on the prediction of new families of TIs and the determination of topological states, mainly using angle resolved photoemission spectroscopy [14], as well as fundamental issues relating to novel spin polarized electronic states [5,7,8]. However, until now, the transport studies that can provide strong direct evidence relating to practical application of the topological insulators have been limited [15–17]. In this Letter, we demonstrate that nanosheets of a Bi_2Te_3 topological insulator several quintuple layers thick display giant and linear magnetoresistance (GLMR). The observation of GLMR paves the way for 3D TIs to be useful for practical applications in magnetoelectronic sensors such as disk reading heads, mechatronics, and other multifunctional electromagnetic applications.

Materials having a zero-energy band gap exhibit fascinating and superior electronic properties compared to materials with a non-zero-energy gap [6]. One of the unique features of the zero-gap materials is that the conductance or resistance is sensitive to external excitations of very low energy, such as electric or magnetic fields, and pressure. The energy required for an electron in the valence band to make a transition to the conduction band can be arbitrarily low in zero-gap materials, leading to finite conductivity under infinitesimal perturbation. Because of the quantum magnetoresistance (MR) effect proposed for materials with zero gap and linear dispersion [18], the MR is expected to be linear, giant, and temperature-independent for zero-gap materials with Dirac linear dispersion, which is ideal for practical applications. One typical example is the observation of giant and linear quantum magnetoresistance in nonmagnetic graphene [19] and disordered induced zero-gap semiconductors such as $Ag_{2\pm\delta}Se$ and $Ag_{2\pm\delta}Te$ [20] and Sb-rich InSb [21].

It also should be noted that a magnetic field can affect the linear dispersion of the 3D TI surface states. For an in-plane field, the Dirac cone state can persist with the Dirac point shifting in the plane [22], causing no change in the Fermi level and little change in the resistivity. Very little change in the in-plane MR has been observed in 2D topological HgTe/CdTe quantum wells and Bi_2Te_3 nanowires or nanoribbons fabricated by using the chemical method for a field parallel to the current direction [23].

However, it should be noted that a gapless surface state with a helical spin state can become gapped in a perpendicular magnetic field, but time-reversal symmetry and

linearity can still be retained in a low field based on the following facts. It has been theoretically predicted that a magnetic field along the z axis can break time-reversal symmetry, induce a gap, and reduce the local density of state in 3D TIs [22]. This defines a sharp criterion to distinguish the TI surface from other two-dimensional systems with an even number of Dirac cones, such as graphene [22,24]. The magnetically induced gap with a field along the z axis was indeed observed experimentally in magnetically doped Bi_2Se_3 crystals by angle resolved photoemission spectroscopy [25]. As a consequence, there are two significant implications that are beneficial to MR for an out-of-plane magnetic field: (i) the surface state will change from metallic to insulating, leading to giant changes in conductance; (ii) the linear energy dispersion surviving in the gap state would cause linear MR. In a Bi_2Te_3 TI, the Dirac cone point of the surface state is located below the Fermi level of the bulk state. These facts have motivated us to measure and expect to achieve giant and linear MR with a magnetic field perpendicular to, rather than parallel to, the ab plane.

The common problem hindering observation of the surface state in Bi_2Te_3 is the metallic state from its bulk due to extra charges from crystal imperfections, dopants, or deficiencies. Therefore, sample thickness is crucial for the expected giant magnetoresistance, since the topological surface state exists only in a few quintuple layers (QL, 1 QL $\approx$ 1 nm) in 3D TIs. It has been reported that the topological surface state appears when the thickness is greater than 2 QL in epitaxial Bi_2Te_3 thin films grown by molecular-beam epitaxy [26]. As for Bi_2Te_3 bulk crystals, generally, the thinner the sample, the greater the proportion of surface states that is expected. Recently, MR in Bi_2Se_3 thin films (3–8 nm) has been reported [27]. It was found that MR increases in thinner films. More importantly it was revealed that linear MR disappears in films of thickness $<$6 nm, due to a gap opening in the surface state induced by the intersurface coupling.

Note that it has very recently been observed by using angle resolved photoemission spectroscopy that the topological state can stay within 7 QL of the surface of a Bi_2Te_3 bulk single crystal [28]. More importantly, the topological state is robust after exposure of samples to N_2 or air at room temperature. However, the surface gapless state was absent in Bi_2Te_3 nanoplates with a thickness of less than 5 nm [29]. As platelike samples have two faces, sample thickness should be greater than 14 QL in order to have a bulk gap state which can secure the topological gapless surface state.

Bulk crystallinity is another important factor affecting the topological state. Poor crystallinity with many crystal defects is the main reason for the bulk metallic state in Bi_2Te_3. Nanoribbons and nanowires of Bi_2Te_3 or Bi_2Se_3 with a thickness of a few QL can be achieved by chemical methods [16,17,29]. Any nonequilibrium growth in the chemical reaction can cause crystal imperfections both at the surface and inside the bulk, masking the intrinsic surface topological states. In comparison, bulk Bi_2Te_3 crystals grown through a slow solidification have better crystallinity, which can be retained by careful mechanical cleavage. However, the thicknesses achieved by mechanical cleavage are usually more than 100 μm, as reported for Bi_2Te_3 crystals [15]. Motivated by the above-mentioned two factors, we used large pieces of single crystals of Bi_2Te_3 cleaved from ingots grown by a slow solidification process as precursors for making high quality nanosheets. Samples with a thickness of 20 nm, corresponding to about 20 QL layers, were used for measuring MR.

Our Bi_2Te_3 nanosheets were produced by so-called liquid exfoliation of layered material, as reported in Ref. [30]. In brief, high purity Bi_2Te_3 single crystals were first crushed into small pieces or powders. Then, the broken pieces or powders were dispersed in N-methyl-pyrrolidinone or acetone in a low concentration of 1 mg/ml by low power sonication for 2 h. A dark gray dispersion was obtained. After being centrifuged at 1000 rpm for 2 h, the top of the dispersion was collected by pipette and was further sonicated by using a point sonic probe for 2 h. After sonication, the dispersion was centrifuged at 1500 rpm for 1 h. The top of the Bi_2Te_3 nanosheet or nanoplate solution was finally collected. The Bi_2Te_3 nanosheets were transferred onto a 300 nm SiO_2/p^{++} Si substrate by a pipette. A standard four-probe electrode (200 nm in width) pattern was defined by the electron beam lithography technique. Ti/Au electrodes (10/40 nm in thickness) were then deposited on the nanosheets.

The structure and chemical composition of the as-prepared Bi_2Te_3 nanosheets were investigated by transmission electron microscope (TEM) (JEOL-2200FS equipped with energy-dispersive x-ray spectroscopy). The surface morphology and thickness of the nanosheets were examined by atomic force microscopy (AFM) (Asylum Research MFP-3D) at room temperature. The magnetotransport measurements were carried out by using a 14 T physical properties measurement system (14 T PPMS, Quantum Design) from 2 to 340 K in fields up to 13 T. The standard four-electrode configuration was fabricated for transport measurements, which is shown as a schematic in Fig. 1(b). The size of the Bi_2Te_3 nanosheet represented is 3.5 μm in length and 2.5 μm in width. During the transport measurement, a constant current of 0.15–0.5 μA was applied through the two outer electrodes. The voltage signal across the inner two electrodes was collected to determine resistance.

The dimensions of the flakes were found to range from hundreds of nanometers to several microns in lateral size, as shown in Fig. 1. Figure 1(c) shows an AFM image of a typical flake with multilayer structure. The high-resolution TEM image of a similar flake is shown in Fig. 1(d),

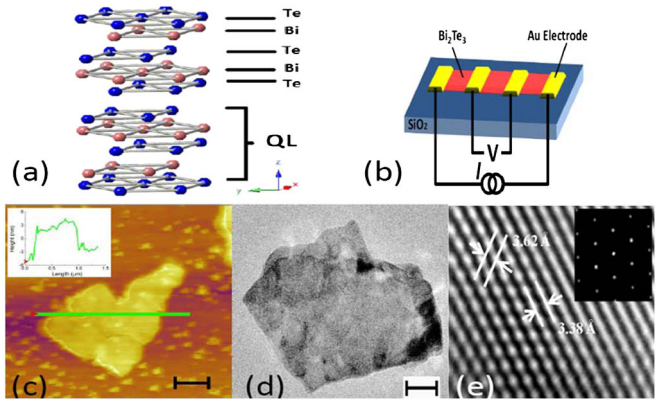

FIG. 1 (color online). Characterization of Bi_2Te_3 nanosheets: (a) Crystal structure of Bi_2Te_3. A QL consists of Te-Bi-Te-Bi-Te layers. (b) Schematic diagram of standard four-probe geometry on nanosheets. (c) An AFM image of a platelike Bi_2Te_3 nanosheet, with the inset profiles corresponding to the green lines in the AFM image. (d) Low-resolution TEM image of a Bi_2Te_3 nanosheet. (e) High-resolution TEM image of the nanosheet edge; the inset is the selected area electron diffraction pattern. The scale bars in (c) and (d) are 200 and 50 nm, respectively.

confirming the high single crystallinity of the Bi_2Te_3 nanosheet. The atomic plane spacings which are marked in Fig. 1(e) correspond to the atomic planes (012) and (104) in the Bi_2Te_3 crystal structure. Generally, larger pieces tended to be thicker than smaller ones. In most cases, steps appear in the height profile, which indicate the multilayer structure of the nanosheet. These steps are in the range of 9.1–21.2 nm, which correspond to 9–21 QL of Bi_2Te_3. It is found that Bi_2Te_3 flakes prepared in *N*-methyl-pyrrolidinone solution are much smaller than those fabricated in acetone. In addition, the *N*-methyl-pyrrolidinone–based nanosheets tend to fold, forming nanotubes or crumpled structures. This is probably because different surface tensions of solvents tend to result in different exfoliating capabilities.

Transverse magnetoresistance was measured in a magnetic field perpendicular to the direction of current. The temperature dependence of the resistance for a Bi_2Te_3 nanosheet 20 nm in thickness, corresponding to 20 QL, was measured between 2 and 300 K in zero field and 13 T, as is plotted in Fig. 2(a). The nanosheet exhibits a slight increase in resistivity at zero field when the temperature decreases, which indicates that the bulk nature is nonmetallic and therefore likely to secure the topological surface state. It is remarkable that the resistance increased significantly over the wide range of temperature from 2 up to 300 K when it was measured in 13 T. The *R*-*T* curve at 13 T is far above the one measured at zero field. The temperature dependence of the MR ratio, defined as $\{[R(H) - R(0)]/R(0)\} \times 100\%$, where $R(H)$ and $R(0)$ are the resistance with and without the magnetic field H, respectively, is also plotted in Fig. 2(a). The MR is over 400% over the wide range of temperatures from 3 up to

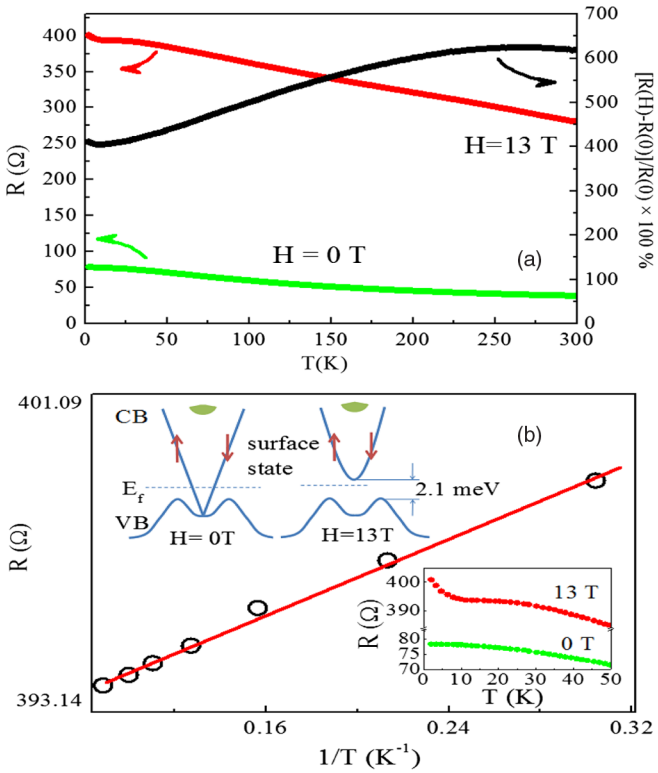

FIG. 2 (color online). (a) Temperature dependence of the resistance and magnetoresistance of a Bi_2Te_3 nanosheet. (b) Arrhenius plot of R vs $1/T$ for low temperatures. Upper left in (b) shows the sketch of the surface state dispersion near the Γ point for 0 and 13 T. Lower right in (b) shows the *R*-*T* curves between 3 and 55 K.

300 K in 13 T. It is remarkable that the MR is over 620% at 300 K. It is interesting to note that the MR reaches a peak of 625% at 280 K and then decreases with decreasing temperature. Also, the MR tends to remain over 600% above 300 K. Furthermore, as we have expected, a gap should be induced by a high magnetic field applied perpendicular to the sample surface. This was clearly evidenced by the clear sharp upturn of the resistance below 10 K, as shown in the inset in Fig. 2(b). The gap value was determined to be 2.1 meV by a linear fitting in the Arrhenius plot [Fig. 2(b)]. This is the first transport evidence for the theoretically predicted gap state induced by a field perpendicular to the surface. The surface state dispersion curves near the Γ point in zero field and 13 T are schematically shown in the inset in Fig. 2(b). In zero field, the Dirac surface state penetrates into the valence band. In the high field of 13 T, the Dirac cone is raised above E_F and leaves a gap of 2.1 meV from the valence band. We notice here that the gap of 2.1 meV is deduced from the low temperature data. The temperature dependence becomes weaker at high temperatures which will result in an effective gap smaller than the bare gap of 2.1 meV. This is because the thermal energy at high temperature is much larger than the gap.

The R vs H between 3 and 340 K in fields up to 13 T (Fig. 3) reveals the following remarkable features of the MR: (i) the MR values above room temperature (340 K) are as high as 600%; (ii) there is no sign of saturation with a field—although similar out-of-plane giant MR has been reported in 2D topological quantum wells [23], it saturated in high fields; (iii) the MR increases linearly with magnetic field for $T < 200$ K and remains linear for $H > 5$ T and $T > 200$ K; (iv) the MR values at high temperatures are greater than those at low temperature for $H > 5$ T; (v) the MR is weakly temperature-independent over the wide temperature range of 200–340 K.

Giant positive and linear magnetoresistance has been observed in two nonmagnetic narrow-band semiconductors, $Ag_{2\pm\delta}Se$ and $Ag_{2\pm\delta}Te$, which have highly disordered stoichiometry [20]. Abrikosov proposed that the disorder induced by nonstoichiometry can transform a narrow-gap semiconductor into a zero-gap state with a Dirac-cone–like linear energy spectrum in both the valence and conduction bands [18]. Only one Landau level with a linear energy spectrum is assumed to participate in the conductivity for such a zero-gap state induced by nonstoichiometric disorder. In a generic quantum description of galvanomagnetic phenomena, the longitudinal MR is given by [18]

$$\rho_{xx} = \frac{1}{2\pi}\left(\frac{e^2}{\epsilon_\infty v}\right)^2 \ln\epsilon_\infty \frac{N_i}{ecn_0} H, \qquad (1)$$

where n_0 is the density of electrons, N_i is the concentration of static scattering centers, ε_∞ is the dielectric constant at high frequency, and v is band velocity, which is a constant band with linear-k dispersion. This quantum MR is linear down to very small fields and is positive, nonsaturating, and, more importantly, independent of temperature. It should be noted that the magnitude of the fluctuations in mobility caused by disorder rather than the mobility itself can also account for the linear magnetoresistance [31].

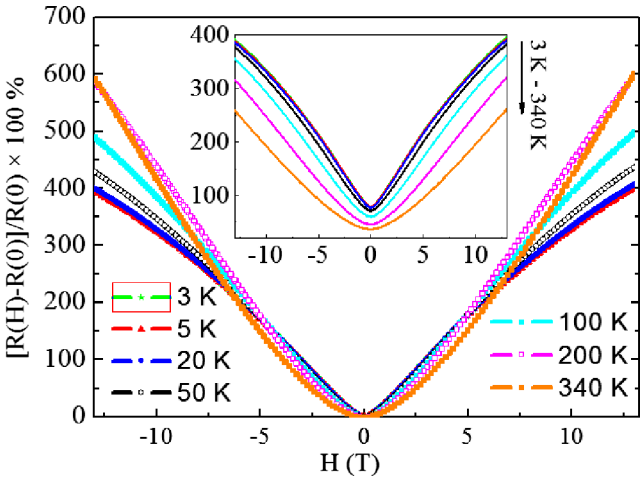

FIG. 3 (color online). Field dependence of the transverse magnetoresistance (inset) and the MR ratio between 3 and 340 K for a Bi_2Te_3 nanosheet.

The GLMR observed in our Bi_2Te_3 nanosheets can be understood by the linear quantum MR model [18], as the topological states are zero-gap with linear E-K dispersion. As we expected, the linear MR comes from the linear energy dispersion of the topological surface state, which can persist at both low and high temperatures. The giant values of over 400%–600% are the clear manifestation of large values of mobility of 2D nondegenerate electrons at the sample surface. The quantum MR have been successfully used to explain the linear magnetoresistance observed in 3D materials such as $Ag_{2\pm\delta}Se$ and $Ag_{2\pm\delta}Te$ [20], narrow-band semiconductors [21], and graphene [19]. The zero-gap band structure with E-K linear dispersion is the key of the Abrikosov model. Such Dirac-like band structure can be realized in either 2D materials or even 3D materials. Disorder (due to disordered stoichiometry) induced linear MR obviously makes no contribution to the observed MR, as it is not the case in our single crystalline Bi_2Te_3 nanosheets. According to the model, the MR should be linear from low to high field and should be temperature-independent. They are indeed temperature-independent for temperatures up to 200 K for magnetic fields less than 6 T (Fig. 3). According to the quantum MR model, as the charge carriers (n_0) may change with temperature, this can account for the weakly temperature-independent MR for $T > 200$ K in Fig. 3 and MR at 13 T in Fig. 2(a). Another possible reason for this deviation is the small k expansion technique used in Ref. [18] to evaluate the k integration ($k \sim \sqrt{B}$). This technique is most accurate as B is not so large. We would like to mention that the deviation from temperature independence of MR at a high B field has been observed in other systems where a linear E-k relation is firmly established [19,20].

The observed large MR value at room temperature is directly related to the reduced dimensionality of topological insulators. As with other observed properties of TIs, dimensionality plays a crucial role. In TIs, topologically protected surface states become dominant when the thickness is reduced (provided that it is still thick enough such that the two surfaces do not couple). In a thick Bi_2Te_3 sample, Qu *et al.* [15] observed a MR of 200% only at the very low temperature of $T = 2$ K and of only 15% at room temperature. In our Bi_2Te_3 nanosheets, the giant MR of 600% persists at room temperature. This suggests a qualitatively different MR mechanism in our sample at room temperatures. If the dimensionality is reduced as it is in our nanosheet samples, the MR is mainly due to the surface states with linear energy dispersion. This is confirmed by the GLMR that we have observed for our sample. At high temperatures, phonon scattering can affect electrons in the bulk bands. This will cause deviation from linearity and reduction in size of MR. However, the surface state is protected due to the time-reversal symmetry of lattice potential. As a result, the GLMR is preserved in our nanosheet samples up to high temperatures.

It should be noted that the MR which increases with increasing temperature, as observed in our Bi_2Te_3 nanosheet, is quite different from what has been seen in existing magnetoresistive materials, where MR increases with decreasing temperature. This feature makes the Bi_2Te_3 nanosheet beneficial even for applications above room temperature. The observed linear giant magnetoresistance in the nano-Bi_2Te_3 topological insulator paves the way for the TIs to be useful for practical applications in magnetoelectronic sensors such as disk reading heads, mechatronics, and other multifunctional electromagnetic applications. It is expected that giant or colossal and linear magnetoresistance could be further enhanced and be present in other families of 3D TIs with appropriate thickness.

In summary, GLMR was observed in 20 nm thick nanosheets of a Bi_2Te_3 topological insulator. The GLMR achieved is as high as over 600% at room temperature with a trend towards further increase at higher temperatures, weak temperature dependence, and linearity with a field, without any sign of saturation at measured fields up to 13 T. The linearity of the MR can be accounted for by the quantum magnetoresistance model proposed for zero-gap band structures with Dirac linear dispersion. The observed linear giant magnetoresistance paves the way for the 3D TIs to be useful for practical applications. A magnetic field included gap is also observed at low temperature.

The authors thank Professor Shoucheng Zhang from Stanford University for his valuable discussions and critical reading of this manuscript. This work is partially supported by funding from the Australian Research Council under a Discovery Project (DP1094073).

*xiaolin@uow.edu.au

[1] C. L. Kane and E. J. Mele, Phys. Rev. Lett. **95**, 146802 (2005).
[2] B. A. Bernevig, T. L. Hughes, and S. C. Zhang, Science **314**, 1757 (2006).
[3] M. Koenig, S. Wiedmann, C. Brüne, A. Roth, H. Buhmann, L. W. Molenkamp, X.-L. Qi, and S.-C. Zhang, Science **318**, 766 (2007).
[4] L. Fu, C. L. Kane, and E. J. Mele, Phys. Rev. Lett. **98**, 106803 (2007).
[5] J. Moore, Nature Phys. **5**, 378 (2009); Nature (London) **464**, 194 (2010).
[6] X. L. Wang, Phys. Rev. Lett. **100**, 156404 (2008); X. L. Wang, S. X. Dou, and C. Zhang, NPG Asia Mater. **2**, 31 (2010).
[7] M. Z. Hasan and C. L. Kane, Rev. Mod. Phys. **82**, 3045 (2010).
[8] X. L. Qi and S. C. Zhang, Rev. Mod. Phys. **83**, 1057 (2011).
[9] H. Zhang *et al.*, Nature Phys. **5**, 398 (2009).
[10] P. Roushan, J. Seo, C. V. Parker, Y. S. Hor, D. Hsieh, D. Qian, A. Richardella, M. Z. Hasan, R. J. Cava, and A. Yazdani, Nature (London) **460**, 1106 (2009).
[11] Y. S. Hor, A. J. Williams, J. G. Checkelsky, P. Roushan, J. Seo, Q. Xu, H. W. Zandbergen, A. Yazdani, N. P. Ong, and R. J. Cava, Phys. Rev. Lett. **104**, 057001 (2010).
[12] L. A. Wray, S.-Y. Xu, Y. Xia, Y. S. Hor, D. Qian, A. V. Fedorov, H. Lin, A. Bansil, R. J. Cava, and M. Z. Hasan, Nature Phys. **6**, 855 (2010).
[13] L. Fu and C. L. Kane, Phys. Rev. Lett. **100**, 096407 (2008).
[14] D. Heieh, D. Qian, L. Wray, Y. Xia, Y. S. Hor, R. J. Cava, and M. Z. Hasan, Nature (London) **452**, 970 (2008).
[15] D. X. Qu, Y. S. Hor, J. Xiong, R. J. Cava, and N. P. Ong, Science **329**, 821 (2010); Y. S. Hor, D. Qu, N. P. Ong, and R. J. Cava, J. Phys. Condens. Matter **22**, 375801 (2010).
[16] H. Peng, K. Lai, D. Kong, S. Meister, Y. Chen, X.-L. Qi, S.-C. Zhang, Z.-X. Shen, and Y. Cui, Nature Mater. **9**, 225 (2010)
[17] F. Xiu, L. He, Y. Wang, L. N. Cheng, L.-T. Chang, M. R. Lang, G. Huang, X. F. Kou, Y. Zhou, X. W. Jiang, Z. G. Chen, J. Zou, A. Shailos, and K. L. Wang, Nature Nanotech. **6**, 216 (2011).
[18] A. A. Abrikosov, Phys. Rev. B **58**, 2788 (1998).
[19] A. L. Friedman, J. L. Tedesco, P. M. Campbell, J. C. Culbertson, E. Aifer, F. K. Perkins, R. L. Myers-Ward, J. K. Hite, C. R. Eddy, Jr., G. G. Jernigan, and D. K. Gaskill, Nano Lett. **10**, 3962 (2010).
[20] R. Xu, A. Husmann, T. F. Rosenbaum, M.-L. Saboungi, J. E. Enderby, and P. B. Littlewood, Nature (London) **390**, 57 (1997).
[21] J. S. Hu and T. F. Rosenbaum, Nature Mater. **7**, 697 (2008).
[22] Q. Liu, C. X. Liu, C. K. Xu, X. L. Qi, and S. C. Zhang, Phys. Rev. Lett. **102**, 156603 (2009); I. Garate and M. Franz, Phys. Rev. Lett. **104**, 146802 (2010).
[23] M. König, H. Buhmann, L. W. Molenkamp, T. Hughes, C.-X. Liu, X.-L. Qi, and S.-C. Zhang, J. Phys. Soc. Jpn. **77**, 031007 (2008); H. Tang, D. Liang, R. L. J. Qiu, and X. P. A. Gao, ACS Nano **5**, 7510 (2011).
[24] K. S. Novoselov, A. K. Geim, S. V. Morozov, D. Jiang, Y. Zhang, S. V. Dubonos, I. V. Grigorieva, and A. A. Firsov, Science **306**, 666 (2004).
[25] Y. L. Chen, J.-H. Chu, J. G. Analytis, Z. K. Liu, K. Igarashi, H.-H. Kuo, X. L. Qi, S. K. Mo, R. G. Moore, D. H. Lu, M. Hashimoto, T. Sasagawa, S. C. Zhang, I. R. Fisher, Z. Hussain, and Z. X. Shen, Science **329**, 659 (2010).
[26] Y. Y. Li, G. Wang, X.-G. Zhu, M.-H. Liu, C. Ye, X. Chen, Y.-Y. Wang, K. He, L.-L. Wang, X.-C. Ma, H.-J. Zhang, X. Dai, Z. Fang, X.-C. Xie, Y. Liu, X.-L. Qi, J.-F. Jia, S.-C. Zhang, and Q.-K. Xue, Adv. Mater. **22**, 4002 (2010).
[27] Hongtao He, B. Li, H. Liu, X. Guo, Z. Wang, M. Xie, and J. Wang, Appl. Phys. Lett. **100**, 032105 (2012).
[28] C. Y. Chen *et al.*, arXiv:1107.5784.
[29] D. H. Kong *et al.*, Nature Nanotech. **6**, 705 (2011).
[30] J. N. Coleman *et al.*, Science **331**, 568 (2011).
[31] M. M. Parish and P. B. Littlewood, Nature (London) **426**, 162 (2003).